Appl. Phys. A (2016) 122:926
DOI 10.1007/s00339-016-0434-8

Applied Physics A
Materials Science & Processing

Investigation of surface passivation schemes for p-type monocrystalline silicon solar cell

Md. Momtazur Rahman[1] · **Ariful Banna Udoy**[2]

Received: 25 April 2016 / Accepted: 15 September 2016

Abstract This paper represents an experiment to analyze the dark saturation current densities of passivated surfaces for monocrystalline silicon solar cells. The samples are diffused at peak temperatures of 800–950 °C. Basically, symmetrical lifetime samples with different doping profiles are prepared with alkaline textured and saw damage etched (planar) surfaces. After $POCl_3$ diffusion, the phosphorous silicate glass layers are removed in a wet chemical etching step. Several designs are chosen for the determination of the sheet resistance (R_{sh}), the concentration profile for excess charge carrier and the minority carrier effective lifetime of the diffused surfaces. The dark saturation current densities (J_o) and the doping profiles are determined accordingly via quasi-steady state photoconductance decay measurement and electrochemical capacitance–voltage measurement. Three different passivation schemes are investigated as follows: silicon nitride (SiN_x) deposited by plasma-enhanced chemical vapor deposition (PECVD) technique, silicon-rich oxynitride ($SiriO_xN_y$) capped with a PECVD SiN_x layer, and thin thermally grown oxide, capped with a PECVD SiN_x layer.

1 Introduction

Solar energy is the most promising energy sources now a day. Various types of losses effectively limit its energy conversion efficiency. The aim of this research is to obtain such datasets for three different industrially applied passivation techniques and a broad range of phosphorus surface concentrations. For the quality consideration, it is necessary to reduce the surface recombination by decreasing the defect concentration at the surface, which can be done by effective surface passivation. There are two strategies for reducing the recombination velocity at the surface: chemical passivation and field effect passivation. The diode characteristics of a solar cell can be described by the one-diode model (Fig. 1):

$$J_{\mathrm{L}} = J_{\mathrm{ph}} - J_o(\exp[q(V_{\mathrm{L}} + J_{\mathrm{L}} * r_{\mathrm{s}})/(K_{\mathrm{B}} * T)] - 1) \quad (1)$$

Here, V_{oc} is the open circuit voltage (local voltage) at p–n junction, V_{L} is the terminal voltage, r_{s} is the series resistance, T is the temperature, K_{B} is the Boltzmann constant, J_{ph} and J_{L} are the photocurrent and load current, respectively. J_o is the dark saturation current density composed by the dark saturation current density of the emitter J_{oe} and the base J_{ob}. The current through the diode J_o is defined by: In the following, a brief description of the influence of the emitter profile and passivation quality on the parameters is given.

$$J_{\mathrm{d}} = J_o(\exp[q(V_{\mathrm{L}} + J_{\mathrm{L}} * r_{\mathrm{s}})/(K_{\mathrm{B}} * T)] - 1) \quad (2)$$

The series resistance is influenced by the emitter and base resistance, the metal resistivity, the metal–semiconductor contacts, among others. For a small series resistance contribution of the lateral carrier flow in the emitter, the lateral conductivity of the emitter has to be small which requires high doping levels or deep profiles. To keep the contact resistance low, heavy doping is essential to be applied below the contacts. If the emitter doping is too low, low resistivity contact formation is not possible. For example, in the case of screen-printed solar cells, a phosphorous concentration of 10^{20} cm^{-3} is required to achieve a

✉ Md. Momtazur Rahman
md.momtazur.rahman@outlook.com

[1] Institute of Micro and Nano Materials, University of Ulm, Helmholtzstraße 18, 89081 Ulm, Germany

[2] Institute of Electronic Devices and Circuits, University of Ulm, Helmholtzstraße 18, 89081 Ulm, Germany

Published online: 01 October 2016

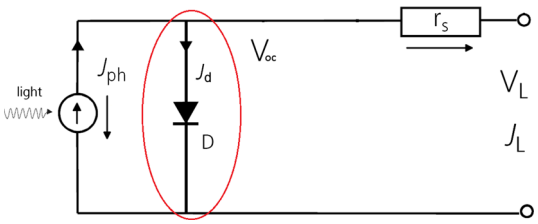

Fig. 1 Equivalent circuit diagram of the one-diode model and the I–V characteristics of the solar cell are given below

low contact resistance between emitter surface and the front metallic contact. The photocurrent can be reduced by the emitter, for example, when carriers are created in the emitter do recombine there and thus do not reach the p–n junction. In this way the emitter serves as an optical filter which should be avoided. These losses are reduced by shallow emitter (less generation in the emitter, shorter distance to p–n junction), low doping densities (longer diffusion length in the emitter) and good surface passivation.

2 Previous work on surface passivation schemes

So many researchers have been doing research on passivated-diffused emitter for last few decades. Comprehensive experimental studies for oxide-passivated phosphorous-diffused emitters have been carried out by King et al. [1] and Sinton and Cuevas [2]. In general, all the experimental studies have been shown that increases in surface phosphorous concentration increase the dark saturation current density (J_{oe}) and textured emitters have typically shown an increase in J_{oe} by a factor of two to three. The increase in J_{oe} being attributed to the increase in surface area of the emitter and the possibility of increased surface recombination on the <111> oriented silicon planes [3]. The experimental data in comparison between furnace oxide passivation and PECVD SiN_x passivation schemes for phosphorous emitters have been published by Aberle [4] and Moschner et al. [5] for the 40 and 90 Ω/sq emitters, respectively. Experimental data for PECVD SiO_xN_y/SiN_x-passivated emitters are less available in the literature. Due to new industrial approach, few works have been reported and Schwab et al. [6] have found improved passivation quality compared to single silicon nitride coating; moreover, silicon oxynitride stack features enhanced light absorption, thereby reducing the short circuit density. The surface passivation properties of thermal SiO_x/SiN_x by plasma-enhanced chemical vapor deposition stacks have been investigated. By annealing these stacks in air, they had achieved surface recombination velocities SRV lower than 2.4 cm/s for thin SiO_2 layers. They had found that the absolute passivation quality of the SiO_2/SiN_x stacks correlates to the SiO_2 thickness [6].

3 Passivated diffused surface

Diffused surfaces are applied in a silicon solar cell to form an emitter or p–n junction. The intention is to collect or separate the photogenerated carriers or to reduce the recombination rate at the metal–semiconductor interface. For the quality consideration, it is necessary to reduce the surface recombination by decreasing the defect concentration at the surface, which can be done by effective surface passivation.

One way of reducing the electron or hole concentration at the surface is by introducing an electric field. Passivation layer (dielectric thin films) with fixed electrostatic charges will repel either electrons or holes, depending on the polarity of the film. This method for reducing the surface recombination velocity (SRV) is referred to as field effect passivation. The field effect passivation depends on the polarity of the charges in the dielectric layer and on the doping at the semiconductor. Silicon oxide layer contains positive charges near the dielectric–semiconductor interface. The polarity and density of the dielectric fixed charges determine the direction and strength of the electric field and hence the extent of field effect passivation. For n-type silicon, the majority of charge carriers (electron) will accumulate at the interface, causing the bands to bend downwards [7] as illustrated in Fig. 2a. By this, an n^+ ^-n region is formed at the surface, in which minority carriers (holes) are repelled, and the total recombination velocity is decreased. The deposition of a passivation layer with fixed positive charges on the p-type silicon material introduces a field effect which depends on the charge density. The dielectric positive charges (passivation layer) will repel the majority carriers (holes) from the p-type silicon, creating a depletion region at this interface as shown in Fig. 2b. Passivation layer with a larger concentration of fixed charges will result in stronger band bending. If the intrinsic energy level E_i bends below the Fermi energy level E_f, the silicon is inverted, and it is switched from p-type to n-type in the interface region, as illustrated in Fig. 2c. In which the n region is separated from the p region by a depletion

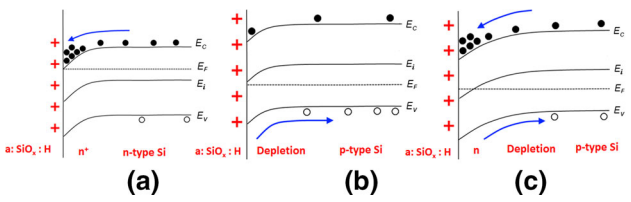

Fig. 2 Band diagrams of doped silicon with positively charged silicon oxide: **a** n-doped silicon with electron accumulation, **b** p-doped silicon with hole depletion and, decreased, **c** p-doped silicon with inversion layer at the semiconductor surface [7]. Here, E_C and E_V are the conduction and valence band edges, E_i is the intrinsic energy level, and E_F is the Fermi level

region. At the metal–semiconductor interface of the silicon solar cell, a high recombination probability is present, which depends on the contact surface area. Though the recombination rate can be minimized by reducing the minority charge carrier density at the highly recombinative metal–semiconductor interface, this can be performed by using a heavy doping and relatively thicker emitter at this regions as explained in [1].

4 Emitter passivation techniques

The emitter passivation has an important influence for high-efficiency silicon solar cells [1]. Most of the solar cells have an emitter at the front surface, and this means that the passivation layer essentially has to be facilitated to reduce the surface recombination and maximize the photogenerated carriers with the compatibility of an anti-reflection coating. In this work, the phosphorous-diffused emitters with three different passivation layers have been investigated. The silicon-rich oxynitride passivation layer ($SiriO_xN_y$ or SiriON) consists of a thin amorphous silicon and hydrogen-rich silicon oxynitride at the bottom layer (8–10 nm) and a SiN_x capping (60 nm) layer on top of it [6] as shown in Fig. 3. This Passivation layer is deposited with the industrially compatible inline plasma-enhanced chemical vapor deposition (PECVD) technique. To produce this passivation layer, the plasma is excited by 2.45 GHz microwave which is coupled into the reaction chamber with a linear antenna.

For the layer deposition, a stable temperature of 400 °C and a chamber pressure of 0.1 mbar are adjusted. In one hand, a mixture of the reactant gases: monosilane (SiH_4), nitrous oxide (N_2O) and hydrogen (H_2) are used for the silicon oxynitride layer (SiO_xN_y) deposition, using the ratio of reactant gas $[N_2O]/[SiH_4]$ equal to 0.3. On the other hand, during silicon nitride (SiN_x) layer deposition, monosilane (SiH_4) and ammonia (NH_3) are used as reactant gases [6], using the ratio of reactant gas $[NH_3]/[SiH_4]$ equal to 3. Basically, 8–10 nm thin thermally grown oxide (SiO_x), capped with a 60 nm silicon nitride layer (SiN_x) by the plasma-enhanced chemical vapor deposition (PECVD) technique as shown in Fig. 4. The deposition of the silicon nitride layer (SiN_x) is performed at a pressure of ~0.1 mbar and at a set temperature of 400 °C, using the ratio of reactant gas $[NH_3]/[SiH_4]$ equal to 3. In case of the thermal oxide layer deposition, the ratio of the reactant gas $[N_2O]/[SiH_4]$ is equal to 4.

The silicon nitride (SiN_x) layer is deposited at a pressure of ~0.156 mbar and at a set temperature of 400 °C. This passivation layer consists of 70 nm of SiN_x (as shown in Fig. 5) which is deposited by the plasma-enhanced chemical vapor deposition (PECVD) technique using the ratio of reactant gas $[NH_3]/[SiH_4]$ equal to 3.

The process gases then propagate through the tube and exit through the small gas outlet located at the bottom of Fig. 5. The temperature inside the tube is controlled by ten heating zones; five of them are located at the top and the rest at the bottom of the tube. There is still a scientific discussion in order to explain how the gases interact through the tube. The simulation results described in [9] suggest that the turbulence and gas velocity variation are strongly dependent on the specific design pattern of the quartz tube.

5 QSSPC measurement techniques

Now a day, the quasi-steady state photoconductance (QSSPC) technique is widely used for minority carrier lifetime measurement. For the lifetime measurement, the instrument is operating regions based on time dependence of the illumination [10].

The measurement quantities are accessible only as average quantities over the wafer thickness, denoted with a subscript "av" in the following section. The experimental

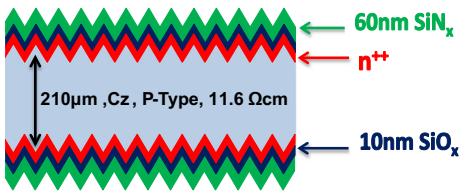

Fig. 4 Industrial thermal oxide passivation layer for textured surface The thermal oxide (SiO_x) passivated surface contains a positive surface field which can repel positive charge carriers from the surface and thus reducing the recombination rate at the surface [8]

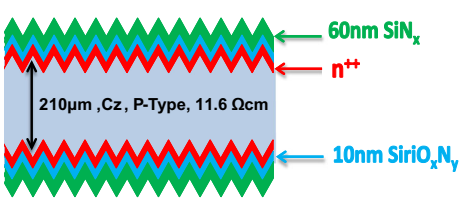

Fig. 3 Industrial $SiriO_xN_y$ passivation layer for textured surface

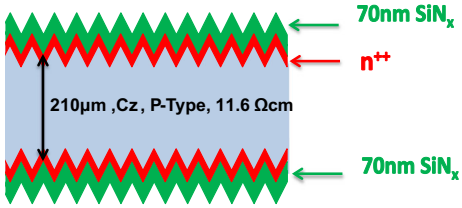

Fig. 5 Industrial silicon nitride passivation layer for textured surface

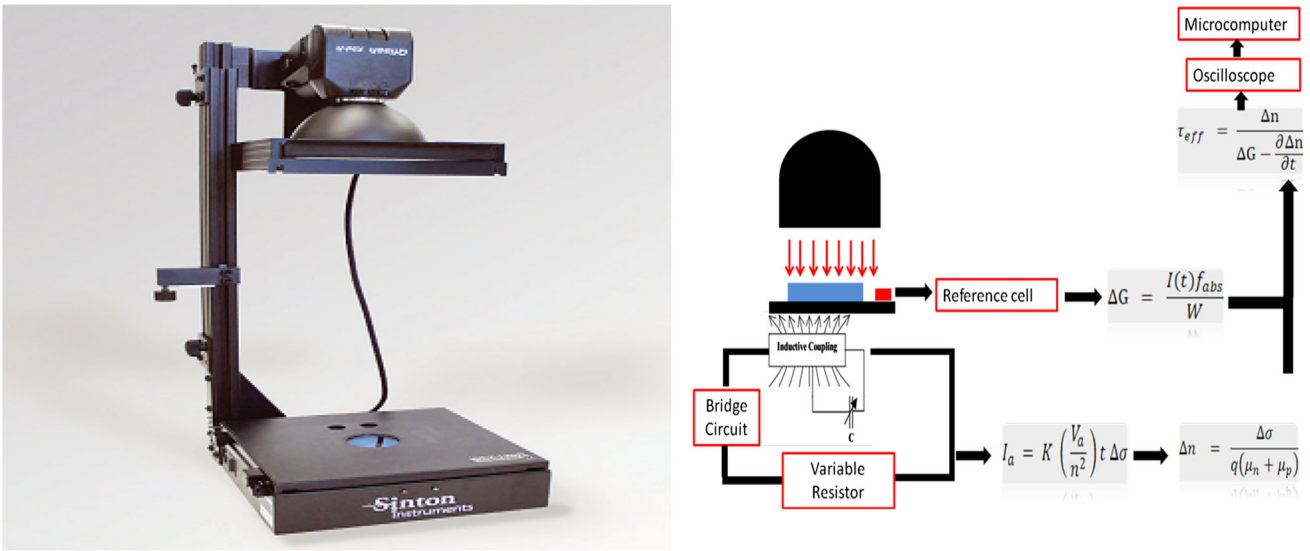

Fig. 6 Schematic of the inductively coupled photoconductance apparatus (e.g., QSSPC) used for measuring the effective lifetime [2]

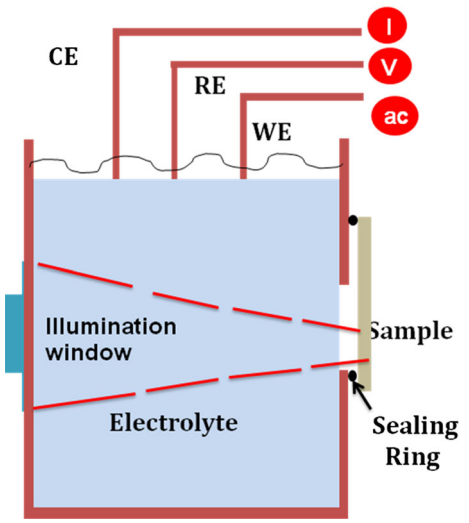

Fig. 7 Schematic diagram of the electrochemical cell showing the platinum (Pt), and carbon (C) electrodes and the pump to agitate the electrolyte [12]

apparatus named QSSPC used in this thesis is fabricated by Sinton Instruments; it is shown in Fig. 6. The sample is kept on the measurement stage (QSSPC instrument) which is inductively coupled with a RF bridge circuit; this circuit can sense the changes of the samples permeability and therefore its conductance. Basically, a reference cell and an oscilloscope are used to determine the illumination $I(t)$ (number of photons per second per unit area) and the excess photoconductance of the sample $\Delta\sigma(t)$, respectively. The excess carrier concentration $\Delta_{\mathrm{av}}(t)$ and the generation rate $\Delta G_{\mathrm{av}}(t)$ of the sample can be determined as follows [11]:

$$\Delta_{\mathrm{av}}(t) = \frac{\Delta\sigma(t)}{q(\mu_{\mathrm{n}} + \mu_{\mathrm{p}})} \tag{3}$$

$$\Delta G_{\mathrm{av}}(t) = \frac{I(t) f_{\mathrm{abs}}}{W} \tag{4}$$

Here, W is the sample thickness, μ_{n} and μ_{p} are the electron and hole mobilities [11], and f_{abs} is the optical absorption coefficient of the sample, normalized to the absorption of the reference cell (Figs. 7, 8, 9).

5.1 First operating region (quasi-steady state mode)

This mode depends on the intensity of the flash which is changing sufficiently slowly so that carrier populations in the sample are always in steady state conditions. Though, this condition is applicable as long as the sample lifetime is lower than the characteristic decay of the xenon flash lamp. The generation rate $\Delta G_{\mathrm{av}}(t)$ can be determined by measuring the light intensity by the reference cell (located on the stage of the QSSPC instrument) and the correction of the reflection and absorption coefficient of the sample. The excess carrier concentration can be created by the illumination, which equals the product of the generation rate and effective lifetime; therefore, the effective lifetime can be calculated as derived in [13]:

$$\tau_{\mathrm{eff}} = (\Delta n_{\mathrm{av}}(t)/\Delta G_{\mathrm{av}}(t)) \tag{5}$$

5.2 Second operating region (transient mode)

In this operating region, carriers are generated by a very short pulse of light and the corresponding decay of the carrier density with time is measured. If the minority

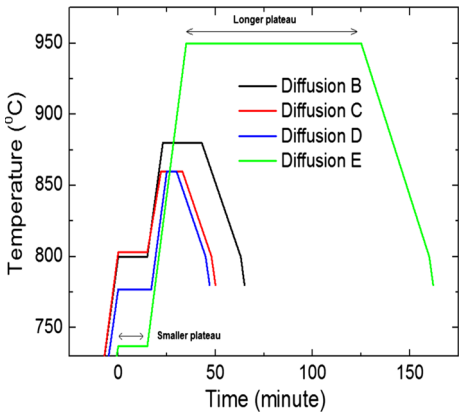

Fig. 8 Schematic recipe of different diffusion profiles. Because the samples are p-type wafers, the n-type emitter region is produced by the diffusion of phosphoryl chloride ($POCl_3$) applying four different recipes. The maximum temperature in this process is in a range of to 850–950 °C. The temperature and time applied at both plateaus can be quite different as is the case of the diffusion E in which the smaller plateau is produced at 737 °C for about 20 min while the longer plateau has a temperature of 950 °C for 90 min. The intention to apply a high plateau in diffusion processes is to segregate the phosphorus silicate glass (PSG) from the silicon surface and also to oxidize the surface to get a lower surface concentration

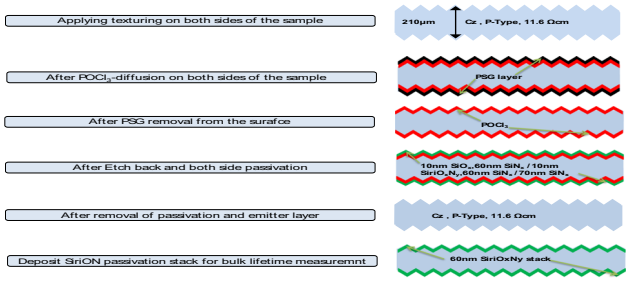

Fig. 9 Major process evolution of symmetrical lifetime samples

carrier lifetime is longer, then the carriers decay slowly. The carrier decay can be described by an exponential decay with time constant τ_{eff}:

$$\Delta n_{\text{av}}(t) = \Delta n_o(t)\exp(-t/\tau_{\text{eff}}) \tag{6}$$

This Eq. (6) leads directly to the measured quantity of the effective lifetime τ_{eff}:

$$\tau_{\text{eff}} = -\Delta n_{\text{av}}(t)/(\mathrm{d}\Delta n_{\text{av}}(t)/\mathrm{d}t) \tag{7}$$

5.3 Third operating region (generalized mode)

Proper analysis of all the possibilities (different mode) requires use of the continuity equation for the excess minority carrier [13]:

$$\frac{\delta\Delta n(t,x)}{\delta t} = G(t,x) - U(t,x) + (1/q)\Delta J_n \tag{8}$$

Here, $G(t, x)$ and $U(t, x)$ are the photogeneration and recombination rate, Δn is the excess minority carrier concentration, q is the elementary charge, and J_{n} is the electron current density. The sample is assumed homogeneous in the directions parallel to the surfaces; the coordinate x denotes the dimension perpendicular to the surfaces.

By varying the illumination level, different operating points can be conveniently explored in this region. In the case of spatially uniform photogeneration, the electric filed in the sample is zero (since the surface recombination zero), and then the carrier concentration remains spatially uniform [14]. By varying the illumination level, different operating points can be conveniently explored in this region. In the case of spatially uniform photogeneration, the electric filed in the sample is zero (since the surface recombination zero), and then the carrier concentration remains spatially uniform. Hence, the last term on the right-hand side of Eq. (8) vanishes. Using the classic relationship $U = \Delta n/\tau_{\text{eff}}$ between the recombination rate and effective carrier lifetime, equation can be written as (9).

$$\tau_{\text{eff}} = \Delta n_{\text{av}}(t)/(\Delta G_{\text{av}}(t) - \partial\Delta n_{\text{av}}(t)/\partial t) \tag{9}$$

To determine the effective lifetime from Eq. (9), it is necessary to measure the time dependence of the excess carrier concentration and the generation rate. A popular method to do this is based on measuring the samples excess photoconductance.

$$J_0 = (qW/2)(\mathrm{d}/\mathrm{d}\Delta n)\left(n_i^2/\tau_{\text{corr}}\right) \tag{10}$$

At the present time, this equation is widely used in WCT-120 lifetime measurement instruments. More information regarding the measurement technique can be found in [15–18].

6 ECV analysis technique

The ECV measurement profiler set two metal contacts on the wafer, and in between these two metal contacts, there is a ring that seals the wafer. The ring forms the opening of the cell that contains certain amount of ammonium bifluoride, and the measuring conditions are regulated by the potential between the semiconductor contacts and the carbon electrode in the electrolyte.

The instrument varies the voltage between the external contacts and the electrode to measure the capacitance of the system. Therefore, a dc potential is given and a small sinusoidal ac signal is overlaid (typically between 100–300 mV at 30–40 Hz) [12]. The capacitance C due to charge increment through space charge region is defined as:

$$C = -\mathrm{d}Q/\mathrm{d}V = qA\frac{\mathrm{d}}{\mathrm{d}v}\int_0^w n\mathrm{d}x \approx qAn\frac{\mathrm{d}w}{\mathrm{d}v} \tag{11}$$

Here, n_n is the charge carrier concentration, A is the interface area (area of the sealing ring), dQ is the charge in the electrolyte, V is the voltage change, and w is the width of the space charge region depending on the voltage

$$w = \sqrt{\frac{2\kappa\varepsilon V}{qn}} \tag{12}$$

To evaluate the profile, the depth of the interface in respect to the original wafer surface has to be known. Therefore, the etch depth has to be calculated. The etching is achieved by dissolving the semiconductor electrolytically. The chemical reaction at the silicon surface introduces a number of free electrons into the silicon, denoted as the dissolution valency Z. On another point of view, Z holes are needed to dissolve one silicon atom. For p-type semiconductors, holes are the majority carriers and dissolution is readily achieved by forward biasing the electrolyte–semiconductor junction. For n-type silicon, the hole is either introduced by a biasing of the junction or created by the absorption of light, which can be controlled during measurement. The etch depth W_R can be calculated from the measured dissolution current I_{diss} using Faraday's law of electrolysis:

$$W_R = \frac{M}{z\,\mathrm{FCA}}\int_0^t I_{\mathrm{diss}}\mathrm{d}t \tag{13}$$

Here, M is the semiconductor molecular weight, Z is the dissolution valency (number of charge carriers required to dissolve one semiconductor atom), F is the Faraday constant (9.64×10^4 C), ρ_w is the semiconductor mass density, and A is the contact area. So, combining Eqs. (12) and (13), the expression for the depth of the measured concentration in respect to the original sample surface X (which is the sum of the etching and space charge depth) can be obtained:

$$\mathrm{X} = W + W_R \tag{14}$$

7 Experimental procedure

To assess the superiority of passivated surfaces for an industrial silicon solar cell, the dark saturation current density (J_o) is calculated ($\Delta n \gg N_A$) by applying the quasi-steady state photoconductance (QSSPC) measurement technique. The samples used in this experiment are monocrystalline p-type samples. The base is precisely doped by boron atom. The wafers are square in size with a dimension of 156×156 mm^2 and a thickness around 210 μm.

7.1 Saw damage etch and texture surface

The first step of the experiment consists on the application of the saw damage etching and texturizing process. When cutting the wafers from the C_z. ingot, a saw damaged layer is generated and needs to be removed at the beginning of the fabrication process to eliminate the surface damages and the possible impurities that might be present from the sawing process. Basically, 20 % concentrated solution of sodium hydroxide (NaOH) is heated up to 80 °C and then the wafer is etched in this solution for about 5 min to remove 4–6 μm of silicon layer from both sides of the wafer. The metallic impurities are further removed by a hydrogen chloride (HCl) bath, and then the wafer is dipped in 2 % concentrated hydrogen fluoride (HF) to make the wafer surface hydrophobic. After going through those steps, the wafer surfaces are much flattened in microscopic scale; therefore, it shows much higher surface reflection. To resemble the front side of monocrystalline silicon solar cells, surface texturing steps are applied at some samples to form a random pyramidal structure. The etchant is heated at a temperature of 78 °C approximately with a chemical mixture of 2 % concentration of potassium hydroxide (KOH), 4 % concentration of isopropyl alcohol (IPA) and water (H_20). In this process, isopropyl alcohol helps to remove the hydrogen bubbles and to form the expected random pyramid structure on the surface. This procedure takes place in a wet chemical bench found in the PV-TEC lab at Fraunhofer-ISE.

7.2 Emitter diffusion

After texturizing, the wafers are cleaned in a wet chemical bench. For this experiment, the corresponding cleaning steps, including HCl and HF dip (only the dipping process is applied because the metal contamination is not significantly high), are applied. The wafers are then dried and loaded to quartz tube boat and fed into the diffusion furnace (to fabricate the emitter region). Four different $POCl_3$ diffusion recipes are applied.

7.3 Etch back

A pretest on additional wafers takes place to estimate the etch rate in order to apply it when etching the symmetrical lifetime samples from this project. Several of the symmetrical lifetime samples were wet chemically etched in an ozone-based solution (composition of 5 g/l O_3, 2 g/l HF and 3 g/l HCl) with an exposure time of 3, 5.3, 8 and

10.30 min. Metal contamination is reduced by using high HCl concentrations. The observed etching rate of textured surfaces is lower than planar surfaces (due to the higher surface area presented at textured surfaces, the surface factor of the textured surface over the planar surface is considered to be 1.6). Moreover, an increase in the ozone concentration results in an increase in the etch rate.

7.4 Passivation

The previous samples are divided into four groups considering the applied diffusion recipe, and then each group is divided into three new groups to apply three different passivation layers in order to shield the base material and to understand its impacts, which leads to analyze the surface recombination properties.

7.5 Contact firing

To simulate the contact firing step and to activate the passivation layer, a temperature of 800 °C is chosen for both, silicon nitride- and thermal oxide-passivated samples while for the case of SiriON-passivated samples, a temperature of 700 °C is selected (in order to maintain the electronic properties of the passivation layer). The belt velocity is around 6200 mm/s and this process last from 4 to 5 s.

8 Results and discussions

8.1 Depth profiles of charge carrier density

In this experiment, the doping profile for phosphorous emitter is measured by means of electrochemical capacitance–voltage (ECV) measurement. Also, the analysis of a wide range of surface concentrations and surface near phosphorous doping is relevant. Therefore four different types of industrial $POCl_3$ diffusions are investigated comprehensively. The aim is to measure different doping profiles and corresponding dark saturation current densities. During the experiment, wet chemical processes, standard cleaning steps and etch back are performed to analyze their influence on the surface concentration. The diffusion profiles are measured by the electrochemical capacitance–voltage (ECV) technique on alkaline saw damaged etched and textured surfaces; these results are shown in Fig. 10 and presented in Table 1. The doping profile differs in surface concentration (1.3×10^{19} cm^{-3}–2.8×10^{20} cm^{-3}) and depth (doping density 10^{16} cm^{-3} at 400–750 nm). The corresponding diffusion recipe E stays longer in situ oxidation compared to diffusion recipe C and D which leads to a deeper profile. Diffusion D exhibits a lower surface concentration and a lower profile due to its lower deposition temperature as shown in Fig. 10.

8.2 ECV measurement analysis

In order to confirm the values obtained from the ECV profile and also to measure the low and deep surface concentration of a finished sample, the etched back process is proposed. As previously explained from Sect. 7.3, the etched back method consists on, when having a sample with its defined carrier concentration at its emitter region; it is then etched several micrometers in order to obtain a lower surface concentration. After the etching process, the ECV profile is obtained once more in which its results are expected to be the same as the one obtained from the same sample before the etching process (non-etch back sample). This consideration takes into account only the region left after the etching process takes place.

9 Artifact correction of ECV profile

When the etched back process removes a portion of the surface, the profile is assumed to be cutoff at a given depth (as explained in the previous paragraph). However, measurement results of etched back samples reveal a decrease in carrier density toward the surface as shown in Fig. 11.

The calculated etched back depth 77 and 129 nm is used in this profile to show the effect. It can be noticed that the charge carrier concentration measured from the etched sample are almost the same as the one obtained from the sample before any etching process took place at any region different than the surface.

The calculated etch depth leads to a good accordance of the profiles. The comparison shows (etched back profiles with the non-etched back profile) clearly that the decrease in charge carrier concentration toward the surface is a

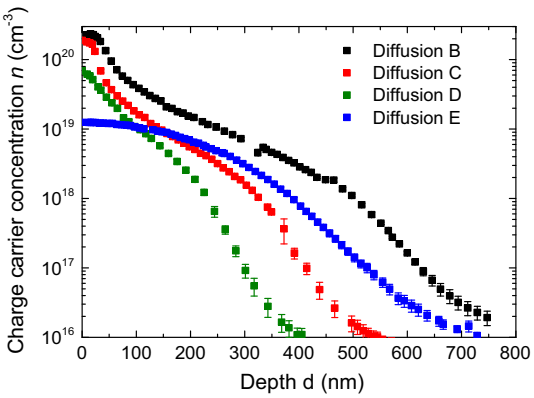

Fig. 10 Electrochemical capacitance–voltage (ECV) profile after phosphorous silicate glass (PSG) etches

Table 1 Diffusion profile parameters

Diffusion type	Surface concentration (cm^{-3})	Diffusion temperature (°C)
B	$2.8 \times 10^{20} \pm 10$ %	803–880
C	$1.9 \times 10^{20} \pm 5$ %	797–860
D	$9.3 \times 10^{19} \pm 10$ %	777–860
E	$1.3 \times 10^{19} \pm 2$ %	737–950

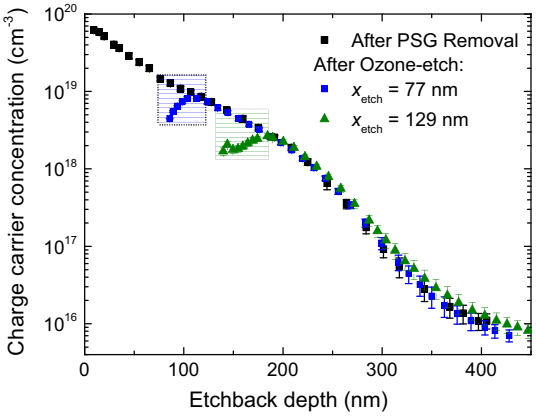

Fig. 11 Carrier concentration profiles measured by ECV technique after the PSG removal (non-etched back) and subsequent etch back of the surface at 77 and 129 nm

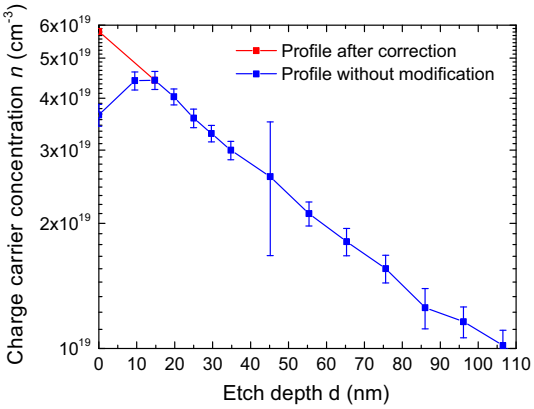

Fig. 12 Carrier concentration over etch depth for an etched back sample. This is an example profile correction of a textured wafer after the diffusion D and PSG etch. The measurement artifact is corrected by simply assuming an exponential extrapolation of the first points decreasing with depth. The *error bars* represent the measurement accuracy of a single ECV measurement

measurement artifact because it is not physically viable. This is because, when applying the etching process, the remaining surface is modified due the chemical residue elements. Here, error bars represent the standard deviation of uncertainty in a reported ECV measurement.

From the previous comparison of the etched back profiles with the non-etched back profile, it can be concluded that the etch depth calculation is very accurate (except at its surface). The measured profiles of the etch back samples in comparison with the non-etched samples go down toward the surface (taking into account its charge carrier concentration) as explained in the previous paragraph, while the one of the later one increases as expected.

10 Modification of ECV profile

The etched back profiles show a good accordance with the profiles of the non-etched back samples apart from the surface near points. As previously discussed, the decrease in carrier concentration toward the surface is a measurement artifact. In order to get the accurate surface concentration of the etched back samples, an adjustment of the carrier concentration toward surface takes place by correcting the profiles assuming an extrapolation of the first decreasing measurement points toward the surface and taking this correction into account for the rest of our calculation as shown in Fig. 12. For the highly doped samples (Diffusion B, C, D), the shape of the profile near the surface is approximately exponential, and thus the extrapolation simply assumes an exponential function through the first three points that are regarded as reliable. For diffusion E, the surface near profile is Gaussian (compare with diffusion with limited doping source and constant diffusion coefficient) in very good approximation, and thus a Gaussian function is applied for the same correction.

At the surface, the measured points will exhibit higher uncertainties in both, SRV and surface concentration calculations as can be described from Fig. 12 by comparing the profile with and without modification.

11 Etch back analysis

In this experiment, several symmetrical lifetime samples with textured and saw damaged etched surface are exposed into an ozone etching solution for different time intervals measuring the resulting etch depth as shown in Fig. 13. In order to compare the difference between a planar (sde) and a textured (txt) surface, diffusion recipes B and D are applied once more at surfaces. As expected, textured surfaces require more etching time in order to reach the same etch depth value from a planar surface due to its higher surface area. In order to compare the difference between a

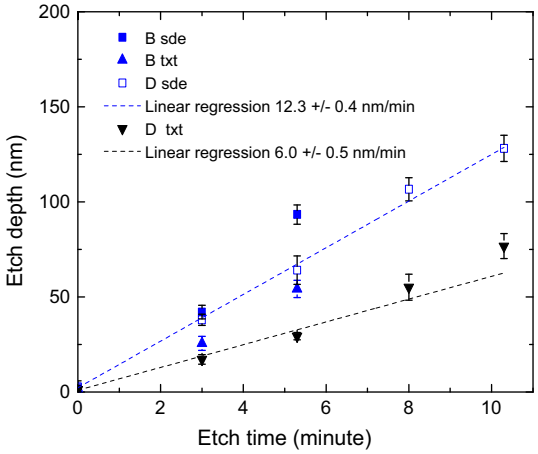

Fig. 13 Calculated etch depth over etching time of the symmetrical lifetime samples for both textured and planar surface. The *error bars* state the standard deviation between different samples. The linear regression for diffusion D leads to an etching rate of 12.3 ± 0.4 nm/min for planar surfaces and 6 ± 0.5 nm/min for textured surfaces. The process shows a higher etch rate on planar surfaces compared to textured surfaces

planar (sde) and a textured (txt) surface, diffusion recipes B and D are applied once more at surfaces). As expected, textured surfaces require more etching time in order to reach the same etch depth value from a planar surface due to its higher surface area .The decrease in sheet conductivity (average conductivity over the etched volume) can be calculated from the measured sheet resistances of the wafer employing the method described in [15]:

$$\sigma_{\text{sh, measureed}} = \frac{1}{2}\left(R^{-1}_{\text{sh, before etch}} - R^{-1}_{\text{sh, after etch}}\right) \quad (15)$$

The decreases in conductivity (as a function of the etch depth $X_{\text{etch-depth}}$) can be calculated from the profile by:

$$\sigma_{\text{sh, calculated}}(X_{\text{etch-depth}}) = \int_0^{x_{\text{etch-depth}}} qN\,(x)\,\mu_{\text{n}}(N,x)\,\mathrm{d}x \quad (16)$$

In which, μ_{n} corresponds to the mobility described in [19], q is the elementary charge and $N(x)$ is the electron density in the emitter region. The etch depth can be calculated by comparing Eqs. (15) and (16):

$$\sigma_{\text{sh, measureed}} = \sigma_{\text{sh, calculated}}(X_{\text{etch-depth}}) \quad (17)$$

The calculated values obtained from Eq. (17) show a linear correlation with the etch time shown in Fig. 13, and therefore the etching rates can be calculated. In the pretest batch, the planar samples from diffusion B and D exhibit an etch rate of 17.5 nm/min. The repetition of the etching procedure with the lifetime samples leads to different etch rates: For diffusion D and planar surfaces, the obtained etching rate is 12.3 ± 0.4 nm/min, but for textured

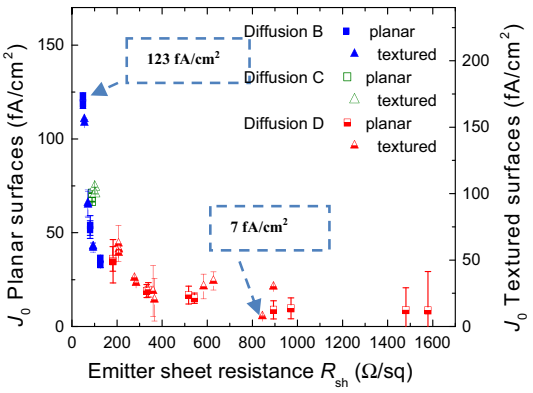

Fig. 14 Analyzed the dark saturation current densities (J_o values) over sheet resistance of the SiriO_xN_y [20]-passivated emitters with a planar and textured surface

surfaces, the etching rate is 6 ± 0.5 nm /min. For all the samples, the etch depth is calculated applying the inductive sheet resistance measurement (R_{sh}) data and electrochemical capacitance–voltage (ECV) profiles of the non-etched back samples. The difference between the pretest and the etching of the lifetime samples is not investigated—presumably the origin lies in slightly different chemical concentrations or temperature of the etch bath.

12 Passivated emitter analysis

12.1 SiriO_xN_y-passivated emitter

The dark saturation current densities (J_o) measured over the sheet resistance of SiriO_xN_y-passivated samples are shown in Fig. 14.

The J_o values increase as the sheet resistance decreases.

12.2 SiO_x-passivated emitter

The measured dark saturation current densities value over sheet resistance of thermal oxide (SiO_2) passivated are shown in Fig. 14. Here, the dark saturation current density (J_o) decreases with an increase in the sheet resistance (R_{sh}). The J_o value increases as the sheet resistance decreases. The J_o values for random pyramid textured samples passivated with thin thermal oxide and PECVD SiN_x.

The lowest J_o values $\sim$ fA/cm^2) of planar samples have been measured for lightly doped emitters while the highest values ($\sim$94 fA/cm^2) for industrial like emitters as the sheet resistance decreases.

Comparing the data for textured and planar samples in Fig. 15, it is revealed that the J_o values increase for thermal oxide-passivated surface when going from planar to a textured surface.

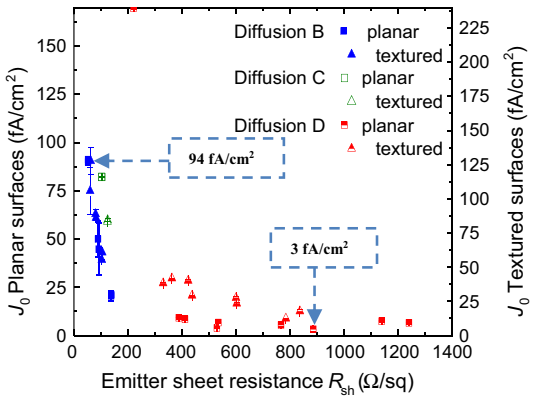

Fig. 15 Analyzed the dark saturation current density (J_o values) over sheet resistance of the thermal oxide [20]. Passivated emitters with a planar and textured surface

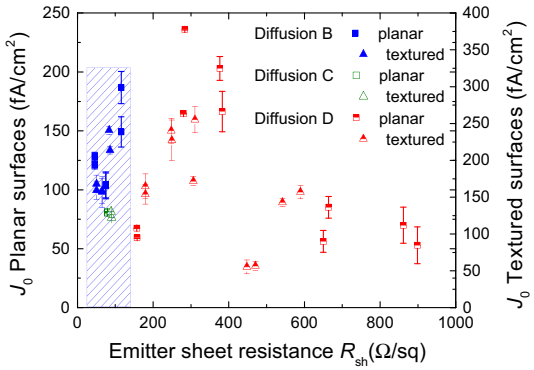

Fig. 16 Analyzed the J_o values over sheet resistance of the SiN_x-passivated emitters with a planar and textured surface. (The measurement values for the textured samples are scaled up on the right-hand side with a factor of 1.6. *Error bars* represent the estimated uncertainty of the J_o analysis)

12.3 SiN_x-passivated emitter

The measured J_o values over the sheet resistance of silicon nitride (SiN_x)-passivated and phosphorous-diffused emitters are shown in Fig. 16. The range of the sheet resistance is covered from 45 to 900 Ω/sq. Particularly, the silicon nitride (SiN_x) passivation was not effective in the experiment (there is no relation between J_o and R_{sh}). Two possible reasons can explain this phenomenon:

1. Contamination of the surface before and after deposition, e.g., during the HF dip.
2. Blistering of the passivation layer during contact firing.

The short contact firing step (applied after the passivation layer has being produced) is good for broadens the surface passivation while the a:SiN_x:H passivation layer with a high silicon content leads to suffer from the blistering effect (formation of bubbles of hydrogen from the SiN_x layer that leads to elevation of the passivation layer

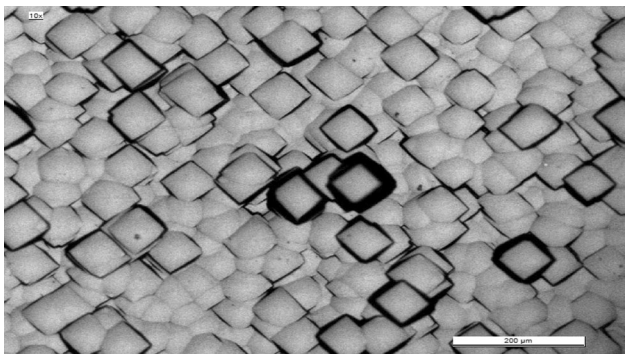

Fig. 17 Optical topography of the SiN_x-passivated surface

from the silicon surface in the extreme case). The blister looks like a hillock which degrades the thermal stability and effective lifetime during firing, and this increases J_o values.

Subsequently, this hydrogen forms complexes with defects in the bulk, and thus within the space charge region. The H-containing species is the reason for the blistering formation. This is not totally confirmed by optical microscopes: There are small points visible (Fig. 17) that could be blisters; however, the density does not appear very high. Optical microscopy cannot reveal bubbles between the passivation layer and the silicon. An optimized composition, annealing time or temperature could avoid the blistering formation. For the same batch, SiN_x passivation layers can be further investigated with improved conditions (e.g., layer thickness, diffusion temperatures).

13 Conclusion

In this experiment, the analysis of the passivation layer quality is presented. To increase the variation in surface concentrations and different profiles, the surface of some samples has been partly removed by etching. To obtain the desired etch depth, a pretest was performed and the etch rate was measured. In this project, the etching rate required to perform the etch back procedure mentioned in the previous paragraph is higher in planar surface compared to textured surface. The mentioned etching rate seems to be reasonable constant, with slight dependencies on the profiles and an increase for high doping concentration.

The dark saturation current density of phosphorus-diffused surfaces is obtained for three different industrial passivation layers (SiriON, SiO_x and SiN_x).The consideration of the relation between J_o and sheet resistance shows that both, the SiriON and SiO_x layers, present good results. In contrast, for the SiN_x-passivated samples, there was no correlation visible. One can follow that in this experiment, the passivation of the SiN_x layers was not effective and the

Table 2 Summary of the results

Sheet resistance, R_{sh} (Ω/sq)	Dark saturation current density, J_o (120 fA/cm^2)	Surface (SDE/TXT)	Diffusion & type	Applications
~49	120	SDE	SiriON, B	Screen-printed contacts
~94	69	TXT	SiriON, B	Evaporated contacts
≥125	84	TXT	SiO_x, C	Non-contacted area

datasets cannot be used for further simulation studies. The origin of the effect is assumed to be the formation of hydrogen bubbles between the passivation layer and the silicon surface or even blistering.

It is demonstrated that both passivation layers present good surface passivation qualities on the $POCl_3$-diffused surfaces. The SiriON and thermal oxide passivation techniques exhibit a reasonable low dark saturation current density even for the case of a high surface concentration (diffusion processes B and D).

Summary of the results cover a broad range of scopes for optimized industrial emitter is mentioned in Table 2.

Acknowledgments Research was conducted at the Institute of Fraunhofer Institute for Solar Energy Systems, Freiburg, Germany. Authors would like to thank Dr. Achim Kimmerle and Dr. Sebastian Mack for helpful discussions and measurement support while performing experimental work. Also authors would like to thank all co-authors and co-workers within the dispensing project as well as our industry partners. Special thanks to Prof. Dr. Ulrich Herr and Prof. Dr. Hans-Jörg Fecht for enlightening me the first glance of research.

References

1. R.R. King, R.A. Sinton, R.M. Swanson, Studies of diffused phosphorus emitters: saturation current, surface recombination velocity, and quantum efficiency. IEEE Trans. Electron Dev. **37**(2), 365–371 (1990)
2. R.A. Sinton, A. Cuevas, Contactless determination of current-voltage characteristics and minority-carrier lifetimes in semiconductors from quasi-steady-state photoconductance data. Appl. Phys. Lett. **69**(17), 2510–2512 (1996)
3. M.J. Kerr, J. Schmidt, A. Cuevas, Comparison of high quality surface passivation schemes for phosphorus diffused emitters. in *Proceedings of the 16th European Photovoltaic Solar Energy Conference*, Glasgow, UK, 2000 (James & James, London, UK, 2000), pp.1715–1718
4. A.G. Aberle, Crystalline Silicon Solar Cells: Advanced Surface Passivation and Analysis of Crystalline Silicon Solar Cells. (Sydney, Australia, 1999)
5. J.D. Moschner et al., Comparison of front and back surface passivation schemes for silicon solar cells. in *Proceedings of the 2nd World Conference on Photovoltaic Energy Conversion* (Vienna, Austria, 1998)
6. C. Schwab et al., Front surface passivation for industrial-type solar cells by silicon oxynitride-silicon nitride stacks. in *Proceedings of the 25th European Photovoltaic Solar Energy Conference and Exhibition* (2010), pp. 2307–2310
7. S. Helland, Electrical characterization of amorphous silicon nitride passivation layers for crystalline silicon solar cells. Thesis, June 2011
8. H. Mäckel, K. Varner, On the determination of the emitter saturation current density from lifetime measurements of silicon devices. Prog. Photovoltaic. **21**(5), 850–866 (2012)
9. B. Mols, R.V.A. Oliemans, A turbulent diffusion model for particle dispersion and deposition in horizontal tube flow. Int. J. Multiph Flow **24**(1), 55–75 (1997)
10. R.A. Sinton, A. Cuevas, A quasi-steady-state open-circuit voltage method for solar cell characterization. in *Proceedings of the 16th European Photovoltaic Solar Energy Conference*, vol. 1152 (2000)
11. J. Krausse, Die Abhängigkeit der Trägerbeweglichkeit in Silizium von der Konzentration der freien Ladungsträger - II. Solid-State Electron. **15**(12), 1377–1381 (1972)
12. D.K. Schroder, Semiconductor material and device characterization, 3rd ed. (Wiley, Hoboken, New Jersey, USA, 2006), p. 790
13. S.M. Sze, Semiconductor Devices: Physics and Technology (Wiley, 2008)
14. H. Nagel, C. Berge, A.G. Aberle, Generalized analysis of quasi-steady-state and quasi-transient measurements of carrier lifetimes in semiconductors. J. Appl. Phys. **86**(11), 6218–6221 (1999)
15. A. Kimmerle et al., Modelling carrier recombination in highly phosphorus-doped industrial emitters. in *Proceedings of the 1st International Conference on Silicon Photovoltaics* (Elsevier Energy Procedia, Freiburg, Germany, 2011), pp. 275–281
16. U. Sinton instrument, WCT120-photoconductance lifetime tester user manual, 2011
17. D.E. Kane, R.M. Swanson, Measurement of the emitter saturation current by a contactless photoconductivity decay method (silicon solar cells). in *Proceedings of the 18th IEEE Photovoltaic Specialists Conference*. (Las Vegas, Nevada, USA, 1985), pp. 578–583
18. M.J. Kerr, P. Campbell, A. Cuevas, Lifetime and efficiency limits of crystalline silicon solar cells. in *Proceedings of the 29th IEEE Photovoltaics Specialists Conference*. (New Orleans, Louisiana, USA, 2002), pp.438–441
19. D.B.M. Klaassen, A unified mobility model for device simulation-II. Temperature dependence of carrier mobility and lifetime. Solid State Electron. **35**(7), 961–967 (1992)
20. M.M. Rahman, H. Mahamudul, M.N. Hasan, Characterization of recombination properties at diffused surfaces for industrial silicon solar cell concepts. Sol. Energy **135**, 215–221 (2016)